PCCP

PAPER

View Article Online
View Journal | View Issue

Cite this: *Phys. Chem. Chem. Phys.*, 2025, **27**, 26131

On the origin of phase transition suppression of P2–$Na_{0.67}MnO_2$ by substitution of Mn with Li

Najma Yaqoob, [ab] Mark Huijben [b] and Payam Kaghazchi *[ab]

Mn-based layered oxides are promising cathode materials for Na-ion batteries, but their low cyclability due to phase transition during charge/discharge remains a challenge. P2–$Na_{0.67}MnO_2$ compound undergoes a severe phase transition of P2 → O2 during charging. It has been proposed that this behavior results from the desodiation-induced change in the Jahn–Teller (J–T) activity of Mn after its oxidation from 3+ to 4+. In this work, we show that the driving force of the phase transition is indeed the oxidation of Mn^{3+} to Mn^{4+} but not the suppression of J–T activity with desodiation. Combining density functional theory calculations and electrostatic analyses indicates that the main factor stabilizing the P2 phase is the Na–Mn interaction, which strongly favors this phase over the O2 phase. Desodiation induced-weakening of this interaction leads to the formation of O2–$Na_{0.11}MnO_2$, which is driven by O–O interaction. Substituting Mn with Li stabilizes P2–$Na_xLi_{0.22}Mn_{0.78}O_2$ even at low Na content (x = 0.11). This is because the Na–Mn interaction is more favorable for the P2 phase, and this energy preference remains almost unchanged after desodiation. The absorption energy of Na at Na sites close to Li_{TM} is much stronger than at sites near Mn_{Mn}, and favors P2 phase. As the overall Na absorption energy (dictated by Na–Mn repulsion) is mainly determined by the nearest Na–Mn neighbor interaction, which does not change much with desodiation, no phase transition to O2 occurs for $Na_xLi_{0.22}Mn_{0.78}O_2$ at x = 0.11. Overall, the phase stability of Na-based layered oxide materials is driven by electrostatic forces, which can be tuned by substitution of Mn by a metal ion of appropriate charge and concentration.

Received 9th July 2025,
Accepted 14th November 2025

DOI: 10.1039/d5cp02620b

rsc.li/pccp

Introduction

After the successful application of Li-ion batteries (LIBs) in portable electronic devices and electric vehicles, significant attention has been directed to sodium-ion batteries (SIBs) because of the low cost and natural abundance of sodium (Na) resources.[1,2] Mn-based layered oxides, $Na_x[M_{1-y}Mn_y]O_2$ (M: metals), are perhaps among the most promising cathode materials because of their low toxicity and high energy density.[3,4] The basic compound Na_xMnO_2 can be classified into P- and O-type depending on the site occupation preference for Na^+, prismatic or octahedral coordination, respectively.[5] The most common layered oxide types are P2 and O3, where the numbers represent the number of distinguishable oxygen layers stacking arrangements per unit cell. Compounds with O3 phases often undergo multiple phase transitions, such as O3–P3–O3′–O1 during charging with a gradual capacity loss during cycling.[6] The P2-type materials generally show a better rate performance and higher initial capacity than O3-type.[7–10] Delmas *et al.*[5] introduced, to our knowledge, the first work on the structural properties of P2–$Na_{0.7}MnO_2$. They found that there is a P2 → O2 phase transition during charging. This behavior decreases the capacity of this compound with cycling and was assigned to the co-operative Jahn–Teller distortion of Mn^{3+}. To solve this issue, Dahn *et al.*[11] substituted Mn with Ni and reported P2–$Na_{0.67}Ni_{0.33}Mn_{0.67}O_2$ with a capacity of 173 mAh g^{-1}. However, the drastic volume change of ∼23% after desodiation, originating from the P2 → O2 phase transition, still decreases the capacity retention of this material. Additionally, Konarov *et al.*[12] reported a reduction in the volume change (∼13%) in P2–$Na_{0.67}Ni_xMn_{1-x}O_2$ by varying the Ni-content from x = 0.0 to 0.2. They found that the P2–$Na_{0.67}Ni_{0.2}Mn_{0.8}O_2$ material shows the best electrochemical performance compared to other Ni contents. The small volume changes in P2–$Na_{0.67}Ni_{0.2}Mn_{0.8}O_2$ was possible because of Ni^{2+} → Mn^{3+} substitution, which can suppress Jahn–Teller distortions. However, suppression of P2 → O2 phase transition during charging is still challenging. In order to enhance the electrochemical properties of P2-type materials, Yabuuchi *et al.*[13] reported that the P2 → O2 phase transition in P2-type $Na_{0.67}Mn_{0.5}Fe_{0.5}O_2$, which showed a reversible capacity of 190 mAh g^{-1} with

[a] *Institute of Energy Materials and Devices, Materials Synthesis and Processing (IMD-2), Forschungszentrum Jülich GmbH, 52425 Jülich, Germany. E-mail: n.yaqoob@fz-juelich.de, p.kaghazchi@fz-juelich.de*
[b] *MESA+ Institute for Nanotechnology, University of Twente, 7500 AE Enschede, The Netherlands. E-mail: m.huijben@utwente.nl*

electrochemically active Mn^{3+}/Mn^{4+} and Fe^{3+}/Fe^{4+} redox processes, is suppressed. However, they found that a reversible P2 → OP4 phase transition occurs at $x = 0.13$ during charging. Bruce *et al.*[14] applied Ni besides Fe to partially substitute Mn, and found that their synthesized cathode material, P2–$Na_{0.67}Ni_{0.17}Fe_{0.33}Mn_{0.50}O_2$, also shows the P2 → OP4 phase transition during charging and less volume change, as compared to the typical P2 → O2 phase transition, which enhances the capacity retention. These previous studies show the importance of doping/substitution to stabilize the P2–Na_xMnO_2 structure by minimizing/reducing the effect of Jahn–Teller distortion in Mn^{3+} and by suppressing the volume change during charging. An improved cycling stability and better capacity retention can be achieved not only by redox-active transition metal substituents such as Ni and Fe but also by electro-inactive elements such as Li and Mg in P2–Na_xMnO_2 structure. Yabuuchi *et al.*[15] reported that the Li-substitution at Mn-sites can suppress the P2 → O2 phase transition in P2–$Na_{0.75}Li_{0.25}Mn_{0.75}O_2$. Density functional theory (DFT) has also been applied to gain further insight into this mechanism. For example, Yang *et al.*[16] studied P2–$Na_{0.67}Li_{0.2}Ni_{0.2}Mn_{0.6}O_2$ using experimental measurements and DFT calculations. They were able to suppress the P2 → O2 phase transition in $Na_{0.67}Li_{0.2}Ni_{0.2}Mn_{0.6}O_2$ upon charging and showed a reversible capacity of 110 mAh g^{-1} over 100 cycles. Their DFT analysis found that the capacity originated from both cationic and anionic redox processes. Further computational studies show that the extraction of sodium ions increases the oxidation state of manganese during charging. This results in a higher concentration of Mn^{3+}, which is prone to Jahn–Teller (J–T) distortions. It has been proposed that these J–T distortions alter the MnO_6 octahedra by changing bond lengths and angles, ultimately destabilizing the P2-structure leading to structural phase transitions.[17,18] Experimental studies have also proposed that the J–T distortion is a driving force of structural instability and phase transition during charging.[19] However, the fundamental mechanism behind the P2 → O2 phase transition in P2–Na_xMnO_2 and the role of low valent substitution (Li^+, Ni^{2+}, and Fe^{2+}) to stabilize the P2 structure during charging/discharging is, however, to our knowledge still unclear and a more detailed understanding is required. In this work, we study the origin of the P2 → O2 phase transition as well as the impact of Li → Mn substitution on the phase stability and transition in P2–Na_xMnO_2. Our DFT-PBE calculation reproduces J–T distortions for $Na_{0.67}MnO_2$ (as also reported earlier by Delmas,[5] Langella *et al.*[17] and Jung *et al.*[18]) and no J–T distortions for $Na_{0.67}Li_{0.22}Mn_{0.78}O_2$, and confirms phase transition in the former and its suppression in the latter case. Our simple electrostatic model without considering J–T distortions also predicts the same trend as DFT which shows the key role of electrostatic interaction rather than J–T distortion on the phase stability. Moreover, for the first time, we also provided a simple quantitative explanation for the phase stabilization (as-synthesized material) and transition (during operation) of P2–$Na_{0.67}MnO_2$ materials with and without Li → Mn substitution, which is an important phenomenon in Na-ion batteries.

Results and discussion

The most favorable atomistic structure for each compound and Na concentration, as well as their corresponding relative electrostatic energies are presented in Fig. 1. We studied the influence of desodiation on the phase stability of Na_xLi_y-$Mn_{1-y}O_2$ materials, by computing the energy difference of P2, O2, and O3 phases as a function of Na ($x = 1.00$, 0.67, and 0.11) and Li ($y = 0$, 0.06, 0.22) concentrations using DFT-PBE (Fig. S1). For the fully sodiated case of $Na_{1.00}MnO_2$, the O3 phase is more favorable than the P2 and O2 phases which agrees with the previous experimental study by Xiaohua *et al.*[20] With a $x = 1.0 \rightarrow 0.67$ decrease in Na concentration, the P2 phase becomes more stable than O3 and O2 phases for Na_xMnO_2 by 13 meV and 23 meV (per formula unit) respectively. Stabilization of the P2 phase has also been reported by experimental measurements from Delmas *et al.*[5] For the desodiation structures, we focused on P2 and O2 phases. After desodiation from $x = 0.67 \rightarrow 0.50$, the P2 phase remains more stable by 15 meV than the O2 phase.

However, after further desodiation the Na_xMnO_2 system undergoes a P2 → O2 phase transition at $x = 0.17$, as the O2 phase is 2 meV more stable than the P2 phase. With a further decrease in Na-concentration ($x = 0.11$), the O2 phase remains more stable than the P2 phase (by 4 meV per formula unit).

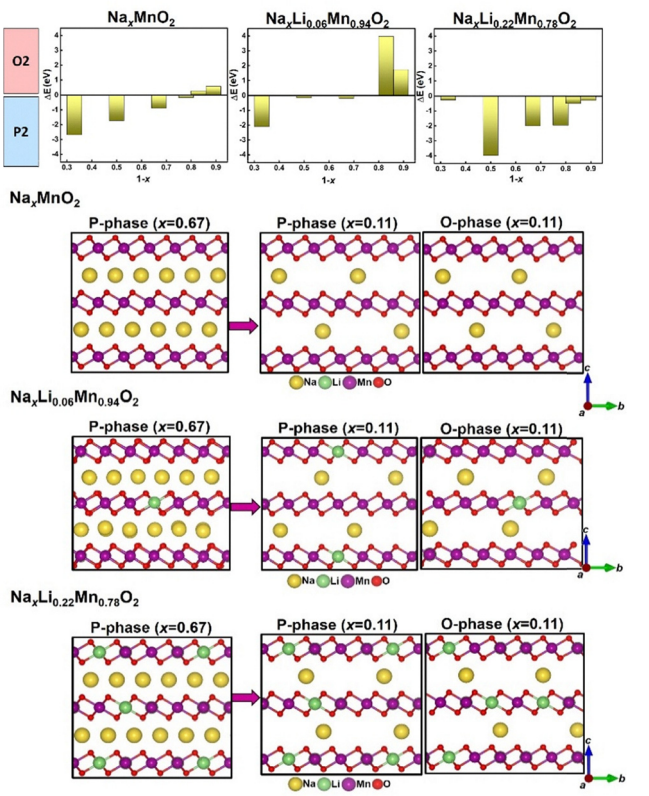

Fig. 1 (top) Computed electrostatic energy difference between the P2 and O2 phase ΔE (eV) = $E_{tot}^{P2} - E_{tot}^{O2}$ *versus* Na-concentration using the Ewald summation (with point charges). (bottom) Side views of atomistic structures.

Our results indicating the P2 → O2 phase transition during charging is consistent with experimental results by Delmas *et al.*[5] and Dahn *et al.*[11] DFT calculations show the following phase transitions to occur for x = 1.00 → 0.67 → 0.50 → 0.17 → 0.11: O3 → P2 → P2 → O2 → O2.

The DFT calculations indicate that in the case of $Na_{1.00}Li_{0.06}Mn_{0.94}O_2$ (Fig. S1), in which 6% of Mn is substituted with Li, the P2 phase is more favorable than the O2 and O3 phases. For the Na concentration of x = 0.67, the P2 phase remains more favorable for Li concentrations of y = 0.06 ($Na_{0.67}Li_yMn_{1-y}O_2$) showing similar behavior to the case of y = 0.0. Furthermore, for $Na_xLi_{0.06}Mn_{0.94}O_2$ (x = 0.67), our DFT-PBE calculation shows that the P2 phase is more stable than the O2 phase by 30 meV (per formula unit) and after desodiation from x = 0.67 to 0.11, a P2 → O2 phase transition occurs and the O2 phase becomes more stable than the P2 phase by 20 meV per formula unit. This means that with 6% Li at Mn sites there is only one phase transition occurring: P2 → P2 → O2 for desodiation of x = 1.00 → 0.67 → 0.11.

After increasing the substitution of Mn by Li to 22% the P2 phase remains the most favorable in $Na_{1.00}Li_{0.22}Mn_{0.78}O_2$ (Fig. S1). For the Na concentration of x = 0.67, the P2 phase forms for Li concentrations of y = 0.22 ($Na_{0.67}Li_yMn_{1-y}O_2$) similar to the cases of y = 0.0 and y = 0.06, which agrees well with experimental measurements by Myung *et al.*[21] However, with such large amount of Li on the Mn sites ($Na_xLi_{0.22}Mn_{0.78}O_2$) there is no phase transition occurring, and the P2 phase is always more stable than the O2 phase by 11 meV and 4 meV (per formula unit) for high (x = 0.67) and low (x = 0.11) Na-concentrations respectively. Experimental studies by Myung *et al.*[21] also show that 22% of Li-doping in Na_xMnO_2 (x = 0.67, 0.11) can suppress the phase transition during charging. The absence of a desodiation-induced phase transition has also been reported by Tarascon *et al.* for $Na_xLi_yMn_{1-y}O_2$ with larger values of y = 0.33.[22] These results indicate a strong influence of Li on the phase stability of $Na_xLi_yMn_{1-y}O_2$.

Our DFT calculations show that the lattice parameter a decreases with a reduction of the Na-concentration from 0.67 to 0.11 for all studied systems (see Table S1 in SI) due to the oxidation of Mn and O, which will be discussed later. The lattice parameter c contracts strongly after desodiation from 0.67 to 0.11 for the cases in which either no Li or a small amount of Li exist at the TM sites ($Na_xLi_yMn_{1-y}O_2$, $y \leq 0.06$), which is because of the phase transition as well as migration of half of the Li cations from TM to Na sites after desodiation. However, the decrease in c parameter in the compound with a high amount of Li at TM sites, namely $Na_xLi_{0.22}Mn_{0.78}O_2$, in which no P2 → O2 phase transition occurs, is very small. The small decrease in c parameter is most likely due to the Li-migration from TM to Na-sites during charging. An experimental study by Tarascon *et al.*[22] on O3–$NaLi_{0.33}Mn_{0.67}O_2$ also indicates Li migration from TM to Na-site during charging and the presence of Li in the Na-layer leads to a decrease in the c parameter with respect to a discharged system which is consistent with our findings. In the discharged state of Li-doped compounds, Li ions occupy TM sites, but upon charging they migrate from TM to Na sites (see Fig. S2 in SI). To determine whether the migrated Li ions from TM to Na sites stay at the Na sites or move to the surface of the cathode during charging, we removed the Li-ions from Na-site in $Na_{0.11}Li_{0.06}Mn_{0.94}O_2$ and $Na_{0.11}Li_{0.22}Mn_{0.78}O_2$ and optimized both structures and lattice parameters. An expansion in the c-value was found for this model, which agrees with the o-XRD measurement by Myung *et al.*[21] This result indicates a spontaneous migration of fractional Li ions from TM to Na sites and subsequent segregation to the surface of $Na_{0.11}Li_{0.22}Mn_{0.78}O_2$. Therefore, we conclude that most of the migrated Li-ions from TM to Na sites do not stay in those Na sites, but segregate to the surface of the cathode consistent with previous study.[21] Therefore, we used $Na_{0.11}Li_{0.03}Mn_{0.94}O_2$ and $Na_{0.11}Li_{0.11}Mn_{0.78}O_2$ to calculate the electronic structure. However, it is important to mention that we calculated electrostatic calculations for both models instead of $Na_{0.11}Li_{0.06}Mn_{0.94}O_2$ and $Na_{0.11}Li_{0.22}Mn_{0.78}O_2$.

Furthermore, the redox mechanism of $Na_xLi_yMn_{1-y}O_2$ were investigated to determine change states of elements for further electrostatic analysis on phase transition, which will be discussed later. To achieve this aim, magnetic moments (represented as number of unpaired electrons (N_{unp})) on elements as well as spin density difference (SDD) plots (Fig. 2 and 3) were computed using DFT-HSE06. The calculated average value of unpaired electrons ($\overline{N_{unp}}$) on Mn in $Na_{0.67}MnO_2$ (Fig. 2) indicates that 36.11% of Mn exhibit a charge state of ~3.8+ ($t_{2g}^3e_g^0$, $\overline{N_{unp}} = 3.24$), and the rest have a charge state of 3.0+–3.3+, from which 44.44% are in the low spin ($t_{2g}^4e_g^0$, $\overline{N_{unp}} = 2.02$), and 19.44% in high spin ($t_{2g}^3e_g^1$, $\overline{N_{unp}} = 3.70$). The formation of Mn^{3+} in the high spin state leads to the Jahn–Teller (JT) distortion as the average axial Mn–O bond lengths ($\bar{d}_{axial}^{Mn}$ = 2.27 Å) are longer than average equatorial Mn–O bond lengths ($\bar{d}_{equatorial}^{Mn}$ = 1.96 Å). A similar Jahn–Teller effect for Mn^{3+} has been reported earlier by Delmas *et al.*[5] With the desodiation of x = 0.67 to 0.11, Mn cations that had charge states between 3.0+ and 3.3+ are oxidized and the average charge state of Mn cations becomes ~3.8+ ($\overline{N_{unp}} = 3.21$).

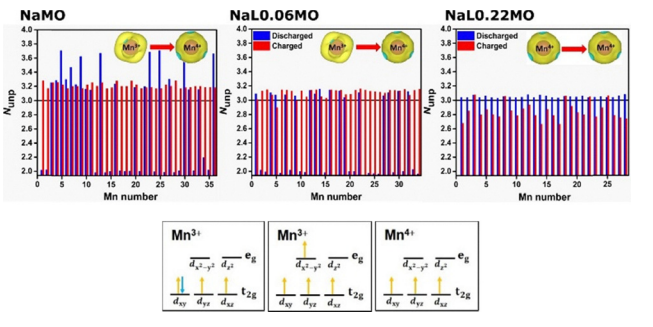

Fig. 2 Calculated number of unpaired electrons N_{unp} on Mn in P2–Na_xMnO_2 (Na_xMO), P2–$Na_xLi_{0.06}Mn_{0.94}O_2$ ($Na_xL_{0.06}MO$), and P2–$Na_xLi_{0.22}Mn_{0.78}O_2$ ($Na_xL_{0.22}MO$) using DFT-HSE06. Inset represents visualization of oxidation state of Mn. Yellow and blue colors represent the up- and down-spin electrons respectively and red arrow represents from discharged to charged state.

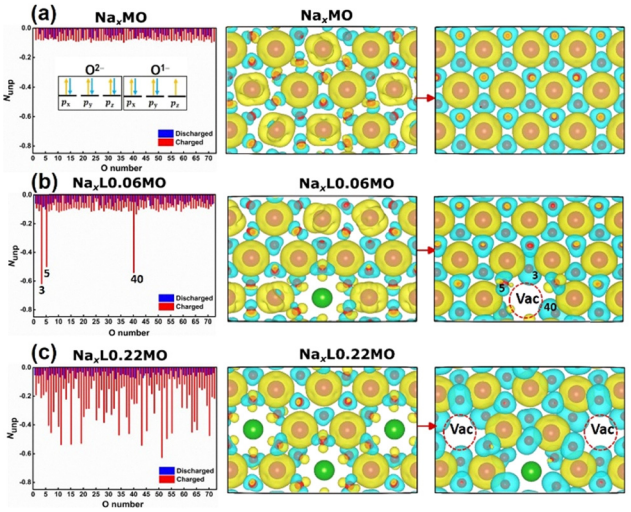

Fig. 3 Calculated number of unpaired electrons N_{unp} of O ions (left figure) and spin density difference (SDD) plots (with an isosurface of 0.006 eV Å^{-3}) of chosen O–TM–O layers of (a) P2–Na_xMnO_2 (Na_xMO), (b) P2–$Na_xLi_{0.06}Mn_{0.94}O_2$ ($Na_xL_{0.06}MO$), and (c) P2–$Na_xLi_{0.22}Mn_{0.78}O_2$ ($Na_xL_{0.22}MO$) with x = 0.67 (middle figure) and x = 0.11 (right figure) using DFT-HSE06. Yellow and blue colors represent the up- and down-spin electrons respectively. The red arrow represents from discharged to charged state.

For $Na_{0.67}Li_{0.06}Mn_{0.94}O_2$, the computed $\overline{N_{unp}}$ for 53% of Mn ($t_{2g}^4e_g^0$, $\overline{N_{unp}} = 1.98$, low spin) and 47% of Mn ($t_{2g}^3e_g^0$, $\overline{N_{unp}} = 3.10$) indicates that Mn cations have an oxidation state of ~3+ and ~4+, respectively. After desodiation of x = 0.67 to 0.11, 53% of Mn cations that had an initial charge state of ~3+ experiences oxidation and exhibits a charge state of ~4+ $\left(\overline{N_{unp}} = 3.11\right)$, which can be clearly seen in the SDD plots (Fig. 3) where the Mn features shrink after desodiation. It is noteworthy that, in comparison to the $Na_{0.67}MnO_2$ compound, the $Na_{0.67}Li_{0.06}Mn_{0.94}O_2$ system shows no cooperative Jahn–Teller distortion in the discharged state but shows phase transition from P2 → O2 during charging of x = 0.67 → 0.11. The computed $\overline{N_{unp}}$ of all Mn cations is 3.05 for $Na_{0.67}Li_{0.22}Mn_{0.78}O_2$ indicating the oxidation state of Mn cations to be 4+ ($t_{2g}^3e_g^0$, $\overline{N_{unp}} = 3.05$). This can also be seen in the SDD plot (Fig. 3) where small features exist on Mn. Upon desodiation from x = 0.67 → 0.11, the calculated $\overline{N_{unp}}$ for Mn remains almost the same, indicating an oxidation state of ~4+.

Compared to $Na_{0.67}MnO_2$, there is no cooperative JT-effect and no phase transition from P2 → O2 for the $Na_xLi_{0.22}Mn_{0.78}O_2$ (for x = 0.67 → 0.11) system as all of Mn shows an oxidation state of 4+ before and after desodiation. Therefore, it seems that this amount of Li acts as a structure stabilizer for $Na_{0.67}Li_{0.22}Mn_{0.78}O_2$ as well as $Na_{0.11}Li_{0.11}Mn_{0.78}O_2$.

The calculated values of $\overline{N_{unp}}$ on O for Na_xMnO_2, $Na_xLi_{0.06}Mn_{0.94}O_2$, and $Na_xLi_{0.22}Mn_{0.78}O_2$ in the discharge state (x = 0.67) are equal to or smaller than −0.05 indicating that the average charge state on O is between 2− and 1.95− (Fig. 3). The small features on O anions in the SDD plot confirm that the charge state of O is close to 2− in the discharge state. Computed $\overline{N_{unp}} = -0.08$ of O in Na_xMnO_2 for x = 0.11 shows only a small charging-induced oxidation of oxygen. Similarly, the O anions in $Na_{0.11}Li_{0.03}Mn_{0.94}O_2$ do not experience much oxidation as the calculated value of $\overline{N_{unp}}$ is −0.12. The oxidation of O in this composition is, however, slightly higher than $Na_{0.11}MnO_2$, which is because of Li for Mn substitution. In particular, some of O anions (*e.g.* O3, O5, and O40) close to the vacant site, which are created after Li migration, undergo the highest oxidations $\left(\overline{N_{unp}} = -0.56\right)$. The larger blue feature on O3, O5, and O40 in the SDD plot of $Na_{0.11}Li_{0.03}Mn_{0.94}O_2$ compared to all O anions in $Na_{0.11}MnO_2$ (Fig. 3) visualize this result. As we discussed earlier, Mn is inactive for $Na_{0.11}Li_{0.11}Mn_{0.78}O_2$, and, therefore, the ion that contributes to the redox mechanism is oxygen. This result is in agreement with previous DFT studies by De la Llave *et al.*[23] and Kim *et al.*[24] who studied P2–$Na_{0.6}Li_{0.2}Mn_{0.8}O_2$ and P2–$Na_{0.67}Li_{0.33}Mn_{0.67}O_2$, respectively, and found extra oxygen states appearing near the Fermi level (in the computed projected density of states) indicating an oxygen anion redox to compensate the charge imbalance. After desodiation of x = 0.67 → 0.11, higher N_{unp} $\left(\overline{N_{unp}} = -0.27\right)$ and larger SDD (more blue features) of O anions close to the vacant site (*e.g.* O6, O7, O10, O11) show that they experience strong oxidation. Higher oxygen redox activity in $Na_{0.11}Li_{0.11}Mn_{0.78}O_2$, as compared to $Na_{0.11}MnO_2$ and $Na_{0.11}Li_{0.03}Mn_{0.94}O_2$, is most likely due to the formation of more 8% TM vacancies in the crystal structure. This triggers oxygen redox reaction as the oxygen anions that have lost their binding to removed Li ions undergo significant oxidation $\left(\overline{N_{unp}} = -0.55\right)$. The sequence of oxygen redox activity in our studied systems from lower to higher is as follows: $Na_{0.11}MnO_2$ → $Na_{0.11}Li_{0.03}Mn_{0.94}O_2$ → $Na_{0.11}Li_{0.11}Mn_{0.78}O_2$. The electrostatic interaction between different cations as well as between them and the oxygen anions might explain the phase stability/transition.

To study this, the differences in total electrostatic energies were calculated using Coulomb energy analysis by using elementary charge states, which balance the system, as well as by applying computed charge states from Fig. 2 and 3 between the P2 and O2 phases (ΔE (eV) = $E_{tot}^{P2} - E_{tot}^{O2}$) for $Na_xLi_yMn_{1-y}O_2$ with different Na (x = 0.67, 0.11) and Li (y = 0, 0.22) concentrations (Fig. 4). The P2 phase is found to be electrostatically more stable than the O2 counterpart for x = 0.67 in all compositions, namely $Na_{0.67}MnO_2$ and $Na_{0.67}Li_{0.22}Mn_{0.78}O_2$. This finding is in line with both our DFT results (Fig. S1) as well as experimental studies on $Na_{0.67}MnO_2$ and $Na_{0.67}Li_{0.22}Mn_{0.78}O_2$ by Delmas *et al.*[5] and Myung *et al.*[21] respectively. Our electrostatic calculation (Fig. 4) for low Na concentrations (charged state) shows that the O2 phase becomes more favorable in the case of Li free, namely $Na_{0.11}MnO_2$ and consistent with DFT calculations and with experimental studies by Delmas *et al.*[5] and Dahn *et al.*[11] However, for the case of high concentrations of Li, namely $Na_{0.11}Li_{0.22}Mn_{0.78}O_2$, the P2 phase remains stable after desodiation, in agreement with DFT and experimental study by Myung *et al.*[21]

Furthermore, we analyzed the pairwise ion–ion interaction by computing their corresponding electrostatic energy differences

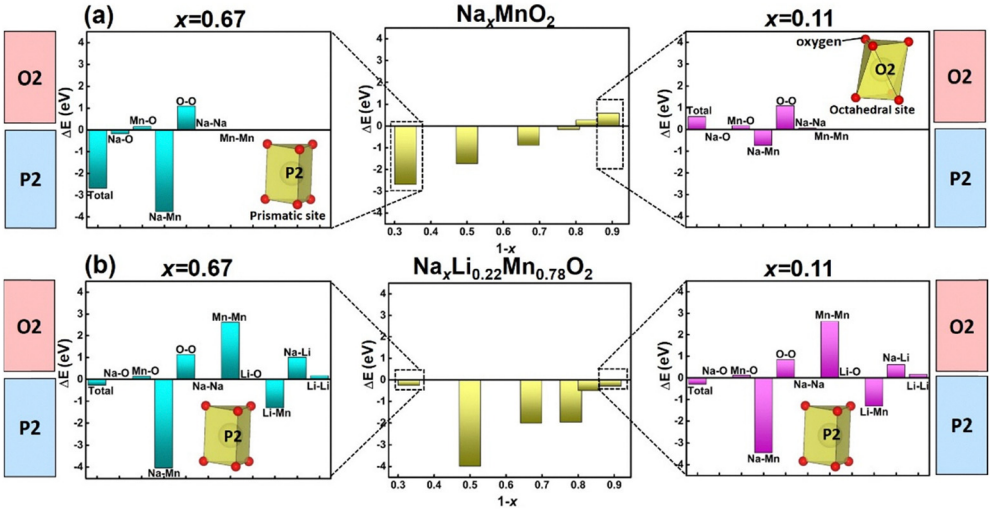

Fig. 4 Computed ΔE is in eV which is the electrostatic energy difference for (a) $Na_{1-x}MnO_2$ (b) $Na_{1-x}Li_{0.22}Mn_{0.78}O_2$ between the P2 and O2 phase *versus* Na-concentration represented in yellow color. Aqua and magenta color represents the discharged and charged state respectively that shows an individual contribution of each element in total electrostatic energy.

between P2 and O2 phases for two compounds with the largest difference in Li and Na concentrations, namely $Na_{0.67}MnO_2$, $Na_{0.11}MnO_2$, $Na_{0.67}Li_{0.22}Mn_{0.78}O_2$, and $Na_{0.11}Li_{0.22}Mn_{0.78}O_2$ (Fig. 4). Moreover, we analyzed pair distribution function (pdf) of ions to determine the underlying mechanism for the phase stability and transition in these materials (Fig. 5 and Fig. S3).

In all cases, the O–O interaction favors the O2 phase, *i.e.* E_{O-O} is lower for the O2 phase. This is most likely due to the shorter distances (r_{O-O}) of nearest neighbors in P2: *e.g.* $r_{peak}(P2) = 3.40$ Å $< r_{peak}(O2) = 3.80$ Å and $r_{peak}(P2) = 4.40$ Å $< r_{peak}(O2) = 4.84$ Å (Fig. S3). With desodiation, the values of ΔE_{O-O} remain unchanged for $Na_{0.11}MnO_2$ (Fig. 4) because of the same oxidation state of O before and after desodiation. However, the O–O interaction changes slightly for $Na_xLi_{0.22}Mn_{0.78}O_2$ ($x = 0.11$) after desodiation because of a very small oxidation of O ($1.95- \rightarrow 1.92-$). The cation–O interactions (cation: Mn, Na, and Li) do not stabilize significantly any of the P2 or O2 phases in both studied systems ($\Delta E_{cat-O} < 0.18$ eV from Fig. 4). Although the Mn–Mn interaction does not stabilize any of these phases for Na_xMnO_2 as $\Delta E_{Mn-Mn} = 0.02$ eV, it does prefer O2 phase over P2 phase ($\Delta E_{Mn-Mn} = 2.62$ eV) for $Na_xLi_{0.22}Mn_{0.78}O_2$, which is probably due to the stronger interlayer Mn–Mn repulsion (as all of Mn become 4+) in the P2 phase after replacing partial Mn by Li cations.

Fig. 4 indicates that the Na–Mn interaction is the determining factor controlling the phase stability of the studied materials. This can be due to the high charge of the Mn cations (from 3.34+ to 4+ depending on the Li and Na concentrations) as well as the distinct phase-dependent Na–Mn separations as discussed later. Since the other pairwise interactions do not change much with desodiation, we will focus on Na–Mn pairs.

The Na–Mn interaction favors the P2 phase in all cases due to the shorter Na–Mn distances for the O2 phase. This can be clearly observed from the pdf plots in Fig. 5. The decrease in the phase stability of the P2 phase over the O2 phase after desodiation in the case of Na_xMnO_2 is probably because of oxidation of Mn from 3.34+ to 4+ (Fig. 2) as well as a decrease in the number of nearest neighbors Na–Mn pairs ($r_{peak}(O2) = 2.73$ Å and $r_{peak}(O2) = 3.20$ Å). However, in the case of $Na_xLi_{0.22}Mn_{0.78}O_2$, the charge states of Mn cations do not change much. Moreover, the intensities of nearest neighbor Na–Mn pairs do not decrease significantly in contrast to the case for Na_xMnO_2. This is because Na ions prefer occupying the Na sites that are closest to the Li ions to reduce the Na^+–Mn^{4+} repulsion. Our DFT calculation shows that these Na sites (shown by Na_{Na}^{LMMM} and Na_{Na}^{LMMLMM} for the O2 and P2 phases, respectively, in Fig. 5) are much more favorable (by 2.82 eV) for Na occupation than the other Na sites that are next to Mn^{4+} (shown by Na_{Na}^{MMMM} and Na_{Na}^{MMMMMM} for the O2 and P2 phases, respectively, in Fig. 5). Therefore, they are the determining sites for the electrostatic energy difference between the P2 and O2 phases. For the aforementioned reasons, the phase stability of the P2 phase over the O2 phase does not change much after desodiation. The similar energy difference between P2 and O2 phases for high and low Na concentrations of the Li-doped case (in spite of their different PDF intensities of next nearest neighbors) confirm our assumption that the interactions between the first nearest Na–Mn neighbors determine the phase stabilities.

We additionally calculated all pairwise interactions for y(Li) = 0.06, 0.11, 0.33, and 0.4 and found that Na–Mn interaction still favors the P2 phase for y(Li) = 0.06, 0.11, and 0.22. With higher Li concentrations of 0.33 and 0.40, the O–O interaction becomes dominant and favors the O2 phase.

As mentioned earlier, there is a Li migration from TM- to Na-sites for $Na_{0.11}Li_{0.06}Mn_{0.94}O_2$ and $Na_{0.11}Li_{0.22}Mn_{0.78}O_2$ structures. We found that for example in $Na_{0.11}Li_{0.22}Mn_{0.78}O_2$, Li at the transition metal (TM) site is 7.96 eV less favorable than that in the Na site. Consequently, after the geometry optimization, Li migrates from the TM site to the Na site. Probably, Li is

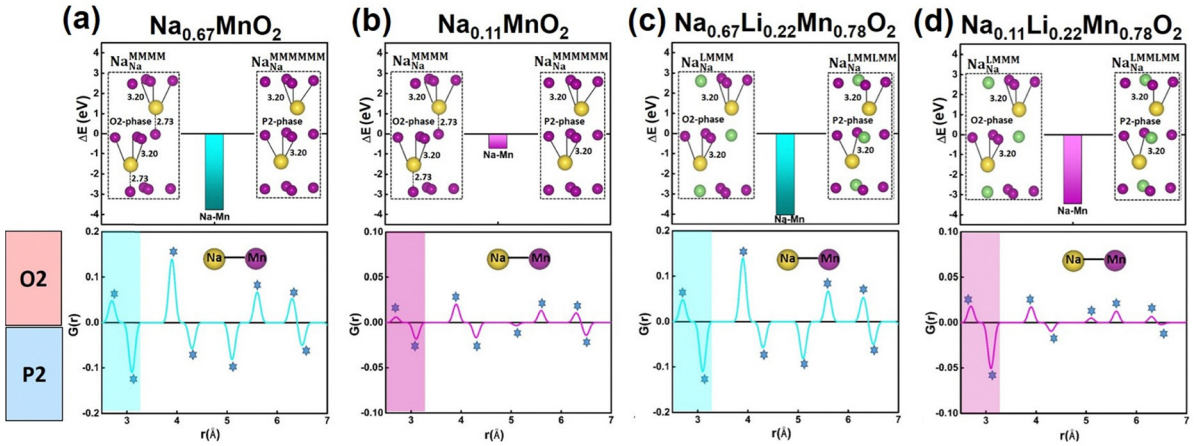

Fig. 5 Calculated pair distribution function which is the difference of O–P ($G_O(r) - G_P(r)$) corresponding to atomic pairs of Na–Mn, inset shows top view of the layer and bond length in angstrom (Å) of (a) $Na_{0.67}MnO_2$, (b) $Na_{0.11}MnO_2$, (c) $Na_{0.67}Li_{0.22}Mn_{0.78}O_2$ and (d) $Na_{0.11}Li_{0.22}Mn_{0.78}O_2$ and shaded area represent the nearest neighbors.

not even stable in the octahedral Na sites due to its small size (compared to Na). Our previous theoretical/experimental study has shown that partially migrated Li to TM sites migrate further to the surface of electrode forming a CEI layer.[21] Therefore, we removed the Li-ions from the Na-sites and studied the phase transition. However, a similar result to the case without Li migration was found: the O2 phase is more favorable than the P2 phase in $Na_{0.11}Li_{0.03}Mn_{0.94}O_2$, while the P2 phase is more favorable than the O2 phase in $Na_{0.11}Li_{0.11}Mn_{0.78}O_2$. Moreover, in these models containing TM vacancies (due to Li migration), Na ions prefer to occupy Na sites next to a TM vacancy to lower the electrostatic energy. A mechanism, similar to $Na_{0.11}Li_{0.22}Mn_{0.78}O_2$ containing Li ions at TM sites, is expected for $Na_{0.11}Li_{0.11}Mn_{0.78}O_2$ containing TM vacancies (created by Li migration) to explain why the P2 → O2 phase transition is prevented.

Method

To obtain the most favorable structures of P2–Na_xMnO_2, P2–$Na_xLi_{0.06}Mn_{0.94}O_2$ and P2–$Na_xLi_{0.22}Mn_{0.78}O_2$, with different x values, we modeled and calculated the total Coulomb energy (E_C) of a large number of likely structures. Total Coulomb energy (E_C) calculations on possible combinations were carried out using the so-called supercell code.[25] We computed electrostatic energies (E_C) for specific elements using the Pymatgen code.[26] By performing DFT-PBE calculation on the electrostatically most favorable configuration, we determined the lowest total energy structure for each Na concentration and used the optimized geometries for further DFT-PBE-D3 and -HSE06 calculations. The total number of considered configurations for E_C calculation and the charge states of ions are discussed in detail in SI. Spin-polarized DFT calculations were performed using the projector augmented wave (PAW) potential method[27] implemented in the Vienna *ab initio* Simulation Package (VASP) code.[28] The Perdew–Burke–Ernzerhof (PBE)[29] form of generalized gradient approximation (GGA) was used for the exchange and correlation potential. The dispersion D3 correction by Grimme[30] was applied to calculate atomistic structures. We have not applied the PBE+U[31] functional for geometry optimization as it is known from previous theoretical works that it does not provide a better description for lattice parameters compared to PBE.[32,33] Performing geometry optimizations with Heyd–Scuseria–Ernzerhof (HSE06)[34] functional is not a common approach to compute the atomistic structure either, because HSE06 is often used for calculating electronic properties such as band gaps and magnetic moments. Moreover, it's computationally expensive and usually doesn't change the structure much compared to PBE.[35] Therefore, it is a more common approach to optimize the geometry with PBE first, then use this optimized geometry and perform single-point calculations with HSE06 functional.[36–38] Therefore, we used HSE06 functional to compute the electronic structure (*i.e.* number of unpaired electrons (N_{unp}) on elements and spin density difference (SDD) plots). Na_xMnO_2, $Na_xLi_{0.06}Mn_{0.94}O_2$, and $Na_xLi_{0.22}Mn_{0.78}O_2$ were modeled by 3 × 6 × 1 supercells with the following number of atoms per supercell: P2–$Na_{0.67}MnO_2$ ($Na_{24}Mn_{36}O_{72}$), P2–$Na_{0.11}MnO_2$ ($Na_4Mn_{36}O_{72}$), P2–$Na_{0.67}Li_{0.06}Mn_{0.94}O_2$ ($Na_{24}Li_2Mn_{34}O_{72}$), P2–$Na_{0.11}Li_{0.06}Mn_{0.94}O_2$ ($Na_4Li_2Mn_{34}O_{72}$) and P2–$Na_{0.67}Li_{0.22}Mn_{0.78}O_2$ ($Na_{24}Li_8Mn_{28}O_{72}$), P2–$Na_{0.11}Li_{0.22}Mn_{0.78}O_2$ ($Na_4Li_8Mn_{28}O_{72}$). Afterwards, we also studied the influence of desodiation on the phase stability of $Na_xLi_yMn_{1-y}O_2$ materials by using a large supercell (3 × 6 × 3) to decrease the uncertainty in the energy differences (Fig. SI). A Gamma-centered k-points mesh of 2 × 1 × 2 and an energy cut off of 500 eV were applied. We performed convergence tests for the energy cut off and k-points sampling (see SI). An electronic and a force convergence criterion of 10^{-4} eV and 2×10^{-2} eV Å^{-1}, respectively, were used for DFT calculations. Atomistic structures and SDD plots were visualized with the VESTA program.[39]

Conclusions

We investigated the origin behind the phase transition in the P2–$Na_{0.67}MnO_2$ cathode by performing DFT calculations and

electrostatic energy analyses. We also simulated the effect of substitution of Mn by Li on the stability of P2–$Na_{0.67}MnO_2$. It is found that the Na–Mn interaction is the most determining factor controlling the phase stability of $Na_{0.67}MnO_2$, which is strongly Na concentration (x) dependent. This pairwise interaction prefers the P2 phase over the O2 phase independent of x value, but this preference weakens with decreasing x. The O–O interaction, which is the second most important parameter determining the phase stability, favours the O2 phase with a very weak Na concentration dependency. For the aforementioned reasons, the preference of the P2 phase due to the Na–Mn interaction becomes weaker than that of the O2 phase due to the O–O interaction leading to the P2 → O2 phase transition in Na_xMnO_2 at low x values (*e.g.* $x = 0.11$). Decrease in the number of nearest neighbor Na–Mn pairs and the oxidation of $Mn^{3.34+}$ to Mn^{4+} after charging are probably responsible for the phase transition. We also explained the reason behind the suppression of the phase transition through the substitution of Mn by low-charge state elements such as Li. It was found that the 22% doping with Li retains the P2 phase during charging. The higher stability of the P2 phase as compared to O2–$Na_xLi_{0.22}Mn_{0.78}O_2$ even after desodiation ($x = 0.67 \rightarrow 0.11$) is dictated by Na–Mn interaction, which is much weaker (more favorable) for Na absorption close to Li at TM sites for the P2 phase. This preference is determined mainly by nearest Na–Mn neighbours which does not change with Na concentration. This work not only quantitatively proves the phase preference in the as-synthesized and desodiated P2–Na_xMnO_2 and P2–$Na_xLi_{0.22}Mn_{0.78}O_2$ but also the corresponding driving force behind the phase stabilities.

Conflicts of interest

There are no conflicts to declare.

Data availability

The data supporting this article have been included as part of the supplementary information (SI). Supplementary information is available. See DOI: **https://doi.org/10.1039/d5cp02620b**.

Acknowledgements

Computation time granted through JARA HPC on the supercomputer JURECA at Forschungszentrum Jülich under Grant No. jiek12 is gratefully acknowledged by the authors. P. K. thanks for the financial support from the ''Deutsche Forschungsgemeinschaft'' (DFG, German Research Foundation) under project No. 501562980.

Notes and references

1 H. S. Hirsh, Y. Li, D. H. S. Tan, M. Zhang, E. Zhao and Y. S. Meng, *Adv. Energy Mater.*, 2020, **10**, 2001274.
2 A. Rudola, R. Sayers, C. J. Wright and J. Barker, *Nat. Energy*, 2023, **8**, 215–218.
3 W. Zuo, A. Innocenti, M. Zarrabeitia, D. Bresser, Y. Yang and S. Passerini, *Acc. Chem. Res.*, 2023, **3**, 284–296.
4 X. Liang, X. Song, H. Sun, H. Kim, M. C. Kim and Y. K. Sun, *Nat. Commun.*, 2025, **1**, 3505.
5 A. Mendiboure, C. Delmas and P. Hagenmuller, *J. Solid State Chem.*, 1985, **57**, 323–331.
6 M. H. Han, E. Gonzalo, M. C. Cabanas and T. Rojo, *J. Power Sources*, 2014, **258**, 266–271.
7 X. Ma, H. Chen and G. Ceder, *J. Electrochem. Soc.*, 2011, **12**(158), A1307.
8 N. Voronina, H. J. Kim, H. M. Shin and S. T. Myung, *J. Power Sources*, 2021, **514**, 230581.
9 L. Zhang, T. Yuan, L. Soule, H. Sun, Y. Pang, J. Yang and S. Zheng, *ACS Appl. Energy Mater.*, 2020, **3**, 3770–3778.
10 N. Voronina, H. J. Kim, A. Konarov, N. Yaqoob, K. S. Lee, P. Kaghazchi and S. T. Myung, *Adv. Energy Mater.*, 2021, **11**, 2003399.
11 Z. Lu and J. R. Dahn, *J. Electrochem. Soc.*, 2001, **148**, A1225.
12 A. Konarov, J. U. Choi, Z. Bakenov and S. T. Myung, *J. Mater. Chem. A*, 2018, **6**, 8558–8567.
13 N. Yabuuchi, M. Kajiyama, J. Iwatate, H. Nishikawa, S. Hitomi, R. Okuyama and S. Komaba, *Nat. Mater.*, 2012, **11**, 512–517.
14 J. W. Somerville, A. Sobkowiak, N. Tapia-Ruiz, J. Billaud, J. G. Lozano, R. A. House and P. G. Bruce, *Energy Environ. Sci.*, 2019, **12**, 2223–2232.
15 N. Yabuuchi, R. Hara, M. Kajiyama, K. Kubota, T. Ishi-gaki, A. Hoshikawa and S. Komaba, *Adv. Energy Mater.*, 2014, **4**, 1301453.
16 L. Yang, L. Y. Kuo, J. M. López del Amo, P. K. Nayak, K. A. Mazzio, S. Maletti, D. Mikhailova, L. Giebeler, P. Kaghazchi, T. Rojo and P. Adelhelm, *Adv. Funct. Mater.*, 2021, **31**, 2102939.
17 A. Langella, A. Massaro, A. B. Muñoz-García and M. Pavone, *ACS Energy Lett.*, 2025, **10**, 1089–1098.
18 H. Jung, J. Kim and S. Kim, *J. Appl. Phys.*, 2022, **5**, 132.
19 C. Wang, L. Liu, S. Zhao, Y. Liu, Y. Yang, H. Yu and J. Chen, *Nat. Commun.*, 2021, **1**, 2256.
20 X. Ma, H. Chen and G. Ceder, *J. Electrochem. Soc.*, 2011, **158**, A1307.
21 N. Voronina, M. Y. Shin, H. J. Kim, N. Yaqoob, O. Guillon, S. H. Song, P. Kaghazchi and S. T. Myung, *Adv. Energy Mater.*, 2022, **12**, 2103939.
22 Q. Wang, S. Mariyappan, G. Rousse, A. V. Morozov, B. Porcheron, R. Dedryvère and J. M. Tarascon, *Nat. Mater.*, 2021, **20**, 353–361.
23 E. de la Llave, E. Talaie, E. Levi, P. K. Nayak, M. Dixit, P. T. Rao and L. F. Nazar, *Chem. Mater.*, 2016, **28**, 9064–9076.
24 D. Kim, M. Cho and K. Cho, *Adv. Mater.*, 2017, **29**, 1701788.
25 K. Okhotnikov, T. Charpentier and S. Cadars, *J. Cheminf.*, 2016, **8**, 17.
26 S. P. Ong, W. D. Richards, A. Jain, G. Hautier, M. Kocher, S. Cholia, D. Gunter, V. L. Chevrier, K. A. Persson and G. Ceder, *Comput. Mater. Sci.*, 2013, **68**, 314–319.
27 P. E. Blöchl, *Phys. Rev. B:Condens. Matter Mater. Phys.*, 1994, **50**, 17953.
28 G. Kresse and J. Furthmüller, *Phys. Rev. B:Condens. Matter Mater. Phys.*, 1996, **54**, 11169.

29 J. P. Perdew, K. Burke and M. Ernzerhof, *Phys. Rev. Lett.*, 1996, **77**, 3865.
30 S. Grimme, J. Antony, S. Ehrlich and H. Krieg, *J. Chem. Phys.*, 2010, **15**, 132.
31 S. L. Dudarev, G. A. Botton, S. Y. Savrasov, C. J. Humphreys and A. P. Sutton, *Phys. Rev. B:Condens. Matter Mater. Phys.*, 1998, **57**, 1505.
32 S. Pakdel, T. Olsen and K. S. Thygesen, *npj Comput. Mater.*, 2025, **1**, 18.
33 C. Franchini, R. Podloucky, J. Paier, M. Marsman and G. Kresse, *Phys. Rev. B:Condens. Matter Mater. Phys.*, 2007, **19**, 195128.
34 A. V. Krukau, O. A. Vydrov, A. F. Izmaylov and G. E. Scuseria, *J. Chem. Phys.*, 2006, **22**, 224106.
35 R. Ramprasad, H. Zhu, P. Rinke and M. Scheffler, *Phys. Rev. Lett.*, 2012, **6**, 066404.
36 J. Paier, M. Marsman, K. Hummer, G. Kresse, I. C. Gerber and J. G. Ángyán, *J. Chem. Phys.*, 2006, **15**, 124.
37 J. Heyd, G. E. Scuseria and M. Ernzerhof, *J. Chem. Phys.*, 2003, **18**, 8207–8215.
38 M. Shishkin, M. Marsman and G. Kresse, *Phys. Rev. Lett.*, 2007, **24**, 246403.
39 K. Momma and F. Izumi, *J. Appl. Crystallogr.*, 2011, **44**, 1272–1276.

